Materials Transactions, Vol. 52, No. 3 (2011) pp. 521 to 525

EXPRESS REGULAR ARTICLE

Effect of Carbon on Spinodal Decomposition in Fe-26Mn-20Al-C Alloys

GowDong Tsay*[1], YiHsuan Tuan*[1], ChihLung Lin*[1], ChuenGuang Chao and TzengFeng Liu*[2]

Department of Materials Science and Engineering, National Chiao Tung University, 1001 Ta Hsueh Road, Hsinchu 30049, Taiwan, R.O.China

The supersaturated austenite (γ) phase decomposed into fine C-rich ordered k′ particles and C-depleted γ_0 phase during quenching in alloys with $5.5 \leq C \leq 8.0$ at%. The misfit between k′ particles and γ_0 phase decreased with increasing carbon content. The strain energy increased dramatically as carbon content approached slightly below 5.5 at%. Undercooling may be insufficient to overcome the strain energy effects, thus leading to the absence of spinodal decomposition and k′ particles in the present and prior austenitic FeMnAlC alloys with $3.1 \leq C \leq 5.2$ at% under the as-quenched condition. Additionally, both the amount of ordered k′ particles and the carbon concentration in the k′ particles increased with increasing carbon content of the alloy. These results revealed that a higher degree of carbon supersaturation in the initial γ phase might promote a tendency toward C-rich k′ particle formation during quenching. [doi:10.2320/matertrans.M2010255]

(Received July 28, 2010; Accepted December 6, 2010; Published February 2, 2011)

Keywords: *spinodal decomposition, ordered k′ particle, X-ray diffraction, transmission electron microscopy, iron manganese aluminum carbon alloy*

1. Introduction

The microstructural developments in fully austenitic FeMnAlC alloys prepared by conventional casting processes have been extensively studied by many researchers.[1–11] In these studies, when an alloy with a chemical composition in the range of Fe-(28–34.3) mass%Mn-(7.8–11.8) mass%Al-(0.74–1.3) mass%C (Fe-(25–30.1) at%Mn-(14.2–20.9) at%Al-(3.1–5.2) at%C) was solution heat-treated in the single austenite (γ) phase (disordered face-centered cubic (fcc)) region and then quenched rapidly, the microstructure of the alloy was single-phase γ.[1–11] When the as-quenched alloy was aged at 500–550°C for moderate periods of time, fine $(Fe,Mn)_3AlC_x$ particles (k′ particles) began to precipitate coherently within the γ matrix.[1–11] The $(Fe,Mn)_3AlC_x$ particle has an ordered fcc crystal structure which belongs to the $L'1_2$ type.[3–8] Recently, we performed transmission electron microscopy observations on the phase transformations of an Fe-30 mass%Mn-9 mass%Al-2 mass%C (Fe-26 at%Mn-16 at%Al-8 at%C) alloy.[12] Consequently, we found that the microstructure of the alloy in the as-quenched condition was γ phase, which contained fine k′ particles formed within the γ matrix by spinodal decomposition during quenching. This is quite different from that observed in the austenitic FeMnAlC alloys with $3.1 \leq C \leq 5.2$ at%, in which fine k′ particles could only be observed in aged alloys.[3–11] This finding suggests that the carbon content may play an important role in the formation of fine k′ particles within the γ matrix during quenching. However, to date, the reason why adding a greater amount of carbon could lead to this result is unclear. Therefore, the main purpose of this work is to study systematically the effect of carbon content on the as-quenched microstructure of Fe-26 at%Mn-20 at%Al-C alloys with $5.0 \leq C \leq 8.0$ at%.

*[1]Graduate Student, National Chiao Tung University

*[2]Corresponding author, E-mail: tfliu@cc.nctu.edu.tw; dir.mse93g@nctu.edu.tw

2. Experimental Procedure

Seven alloys, Fe-26 at%Mn-20 at%Al-C (alloys A (5 C), B (5.5 C), C (6 C), D (6.5 C), E (7 C), F (7.5 C), and G (8 C)), were selected for investigation in the present study. The alloys were prepared in a vacuum induction furnace using pure Fe, Mn, Al, and carbon powder. After homogenization at 1250°C for 12 h under a controlled protective argon atmosphere, the ingots were hot-rolled and then cold-rolled to a final thickness of 2.0 mm. The sheets were subsequently solution heat-treated at 1200°C for 2 h and then rapidly quenched in room-temperature water. X-ray diffraction (XRD) experiments were carried out by using a Bruker D8 model with Cu-K_α radiation operating at 40 kV and 20 mA. Electron microscopy specimens were prepared by means of a double-jet electropolisher with an electrolyte solution of 10 vol% perchloric acid, 30 vol% acetic acid, and 60 vol% ethanol. Electron microscopy was performed on a JEOL-2100 transmission electron microscope operating at 200 kV. The mean size of the fine k′ particles was determined by a LECO 2000 image analyzer.

3. Results and Discussion

Figure 1 shows the XRD profiles of the seven alloys in the as-quenched condition. The profile of alloy A (5 C) reveals only the fundamental $(200)_\gamma$ reflection. However, sideband peaks around the $(200)_\gamma$ reflection could be observed in alloys B (5.5 C) through G (8 C). The peak appearing on the low-angle side was the $(200)_{k'}$ reflection of C-rich k′ particles, whereas that appearing on the high-angle side was the $(200)_{\gamma_0}$ reflection of the C-depleted γ_0 phase.[9] The presence of sidebands demonstrates that the ordered C-rich k′ particles and C-depleted γ_0 phase were formed through spinodal decomposition during quenching in alloys with $5.5 \leq C \leq 8.0$ at%.[5–7,9] Moreover, the intensity of the $(200)_{k'}$ peak increased with increasing carbon content, and the $(200)_\gamma$, $(200)_{k'}$, and $(200)_{\gamma_0}$ peaks all shifted to smaller Bragg angles. This indicates that the amount of k′ particles,

Table 1 Experimental data obtained from the X-ray diffraction profiles of the present seven alloys.

Alloy		A	B	C	D	E	F	G
C at%	Nominal	5	5.5	6.0	6.5	7.0	7.5	8.0
	Virtual	4.98	5.54	6.03	6.52	6.97	7.48	8.02
2θ	k′	—	48.816	48.777	48.722	48.676	48.615	48.468
	γ	49.7	49.600	49.461	49.311	49.192	49.073	48.882
	γ_0	—	50.364	50.125	49.88	49.688	49.511	49.276
Lattice parameter	$a_{k'}$ (nm)	—	0.3728	0.3731	0.3735	0.3738	0.3743	0.3753
	a_γ (nm)	0.3666	0.3673	0.3683	0.3693	0.3701	0.3710	0.3723
	a_{γ_0} (nm)	—	0.3620	0.3637	0.3654	0.3667	0.3679	0.3695
Misfit δ (%)	$\delta_{k'\text{-}\gamma_0}$	—	2.939	2.551	2.192	1.917	1.724	1.557
	$\delta_{k'\text{-}\gamma}$	—	1.486	1.294	1.130	0.994	0.885	0.802
δ^2	$\delta^2_{k'\text{-}\gamma_0}$	—	8.638	6.508	4.805	3.675	2.972	2.424
	$\delta^2_{k'\text{-}\gamma}$	—	2.208	1.674	1.277	0.988	0.783	0.643
Wavelength (nm)		—	12.40	14.20	16.49	18.81	21.18	23.42
$C_{k'}$ (at%)		—	11.08	11.59	12.27	12.78	13.63	15.32
$(FeMn)_3AlC_x$		—	$x = 0.50$	$x = 0.53$	$x = 0.56$	$x = 0.59$	$x = 0.63$	$x = 0.73$

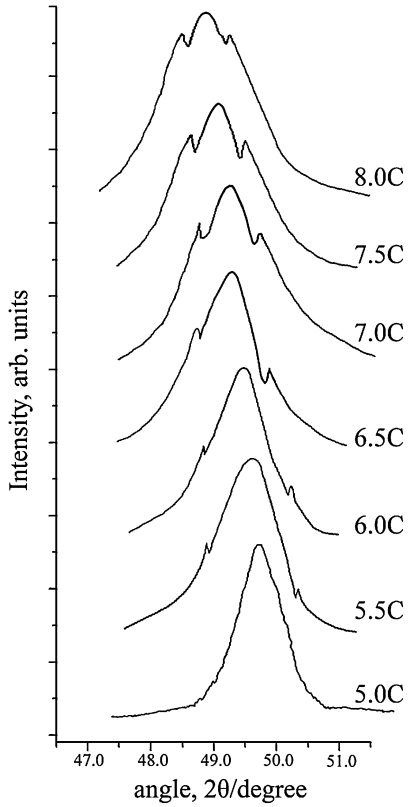

Fig. 1 X-ray diffraction profiles around the $(200)_\gamma$ Bragg reflection for the present seven alloys.

as well as all the lattice parameters of γ, k′ particles, and γ_0 phases, increased with increasing carbon content. It is also shown in Fig. 1 that with increasing carbon content, the sidebands moved closer to the main $(200)_\gamma$ peak, indicating that differences in the parameters between k′ particles and γ_0 phase decreased. The experimental data above measured from the XRD profiles are listed in Table 1. The misfit ($\delta_{k'\text{-}\gamma_0}$) was calculated using the equation:

$$\delta_{k'\text{-}\gamma_0} = 2\left|\frac{a_{k'} - a_{\gamma_0}}{a_{k'} + a_{\gamma_0}}\right| \quad (1)$$

For comparison, the misfit $\delta_{k'\text{-}\gamma}$ was also calculated. Both are listed in Table 1. The modulation wavelength was determined using the Daniel-Lipson equation:[6,9]

$$\lambda = \frac{h a_\gamma \tan\theta}{\Delta\theta(h^2 + k^2 + l^2)} \quad (2)$$

where λ = the average modulation wavelength; θ = the Bragg angle for the γ peak; $\Delta\theta$ = the angular spacing between the sideband and the main $(200)_\gamma$ Bragg peak; and h, k, l = the Miller indices of the Bragg peak (h = 2, and k, l = 0). From Table 1, it is clear that increasing the carbon content causes the misfit to decrease and the wavelength to increase.

Figures 2(a) through (c) show selected-area diffraction patterns (SADPs) of alloys A (5 C), D (6.5 C), and G (8 C), respectively. In addition to the fundamental $(200)_\gamma$ diffraction spot, neither the diffraction spot of ordered k′ particles nor the satellites could be detected in alloy A (5 C). However, both the ordered k′ particle diffraction spot and satellites could clearly be observed in alloys D (6.5 C) and G (8 C). Evidently, spinodal decomposition and formation of ordered k′ particles occurred during quenching. In Figs. 2(b) and (c), it is also seen that in alloy G (8 C), which has a higher carbon content, the $(100)_{k'}$ spot is relatively brighter and the spacing between satellites and the main spot is comparatively smaller. The misfit ($\delta_{k'\text{-}\gamma_0}$) and wavelength ($\lambda$), obtained from measurements of the spacing between the satellites and the main spot along the [100] direction in the SADPs, were 2.24% and 15.7 nm for alloy D (6.5 C), as well as 1.59% and 22.3 nm for alloy G (8 C), respectively. Figures 2(d) and (e) are two dark-field (DF) electron micrographs taken with the $(100)_{k'}$ superlattice reflection in the [001] zone. They reveal that the amount of ordered k′ particles in alloy G (8 C) was significantly greater than that in alloy D (6.5 C). In these figures, it is also seen that fine k′ particles were formed along

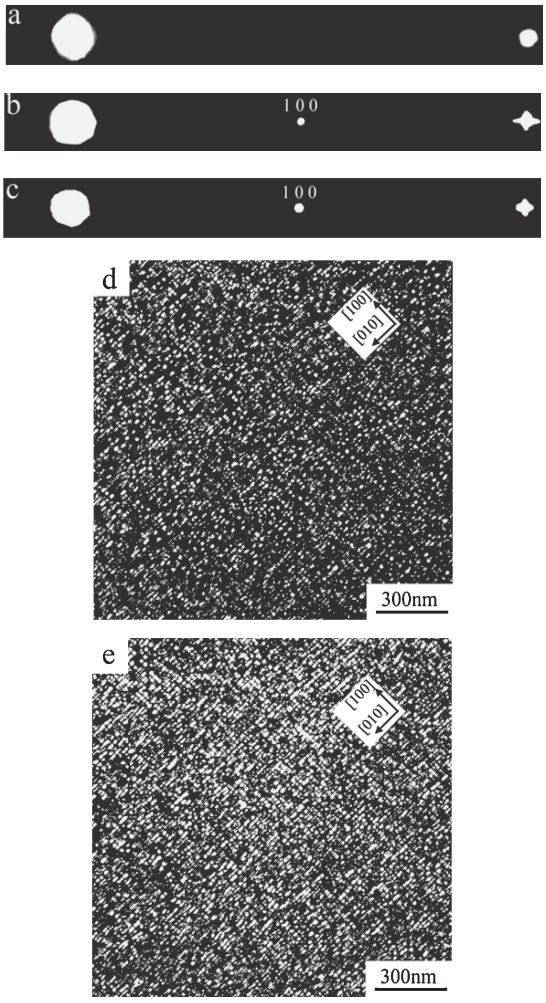

Fig. 2 Transmission electron micrographs of the present alloys in the as-quenched condition. (a)–(c) SADPs of alloys A (5 C), D (6.5 C), and G (8 C), respectively. (hkl: k′ particle), (d)–(e) $(100)_{k'}$ DF images of alloys D (6.5 C) and G (8 C), respectively.

the ⟨100⟩ direction, consistent with the appearance of the satellites along the ⟨100⟩ reciprocal lattice directions in Figs. 2(b) and (c). These results obtained by TEM were in good agreement with those investigated by XRD. Image analyses of Figs. 2(d) and (e) indicated that the mean sizes of fine k′ particles formed in alloys D (6.5 C) and G (8 C) were about 6 and 11 nm, respectively. A detailed TEM examination revealed that although the values of misfit ($\delta_{k'\text{-}\gamma_0}$) in alloys D (6.5 C) and G (8 C) reached 2.24 and 1.59%, respectively, no misfit dislocations could be observed on the interface between the k′ particles and the γ_0 phase. The reason is probably that the fine k′ particles are very small. According to the values of misfit ($\delta_{k'\text{-}\gamma_0}$), the expected distances between two misfit dislocations in alloys D (6.5 C) and G (8 C) were calculated to be about 16.6 and 23.6 nm, respectively, which is much larger than the size of the k′ particles.

Based on the preceding results, some discussion is appropriate. The microstructure of the present alloy A (5 C) in the as-quenched condition was single-phase γ, which is similar to that observed in as-quenched austenitic FeMnAlC alloys with $3.1 \leq C \leq 5.2$ at%.[1–11] However, spinodal decomposition and formation of ordered k′ particles occurred during quenching in the present alloys with $5.5 \leq C \leq 8.0$ at%. Regarding spinodal decomposition, two important factors should be considered: (1) interfacial energy effects, and (2) coherency strain energy effects.[13] The k′ particle is a fcc-based phase of $L'1_2$ ordered crystal structure with a C atom at the body center site, an Al atom at the corner positions, and three (Fe, Mn) atoms positioned randomly at the face center sites in its fcc-based unit cell.[8] On the other hand, γ_0 is a disordered fcc phase with C atoms positioned randomly at the octahedral interstitial sites. As the γ_0 phase and ordered k′ particles have the same fcc-based crystal structure and similar lattice parameters, their interface would be fully coherent. Therefore, only chemical contributions should be considered to the interfacial energy.[13] The carbon concentration in the equilibrium $(Fe,Mn)_3AlC_x$ particles of austenitic FeMnAlC alloys aged at 500–550°C for longer times has been studied by several workers. Consequently, three different values of X have been obtained (0.4, 0.6, and 0.66).[6,9,11] Furthermore, to the authors' knowledge, no information concerning the interfacial energy between the γ_0 phase and ordered k′ particles has been provided in previous studies. Additionally, in the early stage of spinodal decomposition, the composition fluctuation profile exhibited a sinusoidal wave.[6,14] Therefore, a conclusive description of the interfacial energy between the γ_0 phase and ordered k′ particles cannot be given in the present study.

Since the composition ratio of (Fe, Mn) and Al in all of the present alloys approximates that of $(Fe,Mn)_3AlC_x$ particle, it is plausible to suggest that the composition fluctuation was primarily due to the carbon atom. As is evident from the experimental results above, all the lattice parameters of the phases increased with increasing carbon content of the alloy. This suggests that the carbon concentration in these phases increased simultaneously. However, the carbon contribution to the increase in the lattice parameter of the ordered k′ particle is distinctively less than in the disordered γ_0 phase.[15] Therefore, although all the lattice parameters of the phases increased with increasing carbon content, the increment in the disordered γ_0 phase was larger than that in the ordered k′ particles. Consequently, the misfit between the ordered k′ particles and disordered γ_0 phase would be reduced with increasing carbon content, which is consistent with the results obtained by XRD and TEM. To emphasize the characteristics, the variations in the lattice parameters and misfits as a function of carbon content are plotted in Fig. 3. For a fully coherent interface, the coherency strain energy would be roughly proportional to δ^2.[13] In Table 1, it is clearly seen that the $\delta^2_{k'\text{-}\gamma_0}$ in alloy G (8 C) is only 2.424, whereas that in alloy B (5.5 C) is 8.638. This indicates that the strain energy in alloy B (5.5 C) is about 3.56 times that of alloy G (8 C). The average change in $\delta^2_{k'\text{-}\gamma_0}$ between two adjacent alloys ($\Delta\delta^2_{k'\text{-}\gamma_0}/0.5$ at%) was calculated from Table 1. In terms of our calculations, it was found that the values between alloys B (5.5 C)-C (6 C), alloys C (6 C)-D (6.5 C), alloys D (6.5 C)-E (7 C), alloys E (7 C)-F (7.5 C), and alloys F (7.5 C)-G (8 C) were about 4.261, 3.406, 2.260, 1.406, and 1.096, respectively, which corresponds to a ratio of 3.89 : 3.11 : 2.06 : 1.28 : 1. This means that the average increment of strain energy per decrement of at% C between 6 and 5.5 at% C is

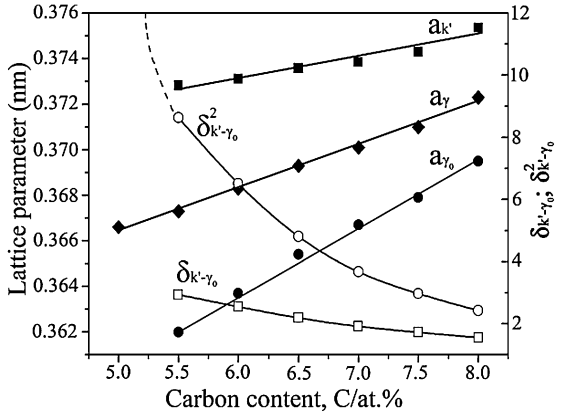

Fig. 3 Variations in the lattice parameters of k′ (■), γ (◆), and γ_0 (●) phases, as well as $\delta_{k'-\gamma_0}$ (□) and $\delta^2_{k'-\gamma_0}$ (○), as a function of the carbon content.

3.89 times greater than that between 8 and 7.5 at% C. The variation in $\delta^2_{k'-\gamma_0}$ with carbon content is also plotted in Fig. 3. The dotted line shows the expected values extrapolated from the $\delta^2_{k'-\gamma_0}$–C plot. It is evident that the slope of the $\delta^2_{k'-\gamma_0}$–C curve increased gradually with decreasing carbon content from 8.0 at% C, and became very steep as the carbon content approached concentrations slightly below 5.5 at%. Accordingly, it is reasonable to expect that a small amount of decrease in carbon content below 5.5 at% would cause the coherency strain energy to increase dramatically. As a result, undercooling may be insufficient to overcome the strain energy effects. Consequently, spinodal decomposition was completely suppressed and not detected in the present alloy A (5 C). In addition, the experimental results revealed that both the wavelength and the amount of ordered k′ particles increased with increasing carbon content. This suggests that the temperatures of both spinodal decomposition and ordering reaction increased with increasing carbon content.

In previous studies, it was seen that when austenitic FeMnAlC alloys with $3.1 \leq C \leq 5.2$ at% were solution heat-treated at 980–1050°C and then rapidly quenched in room-temperature water or ice water, the microstructure was single-phase γ.[1–11] When the as-quenched alloy was aged at 500–550°C, both spinodal decomposition and formation of ordered k′ particles could be detected during the early stage of isothermal aging.[3–11] Han *et al.* proposed that ordered k′ particles nucleate in C-rich zones of the γ matrix after undergoing spinodal decomposition.[4] In contrast to this proposition, Choo *et al.* claimed that spinodal decomposition and formation of ordered k′ particles occurred concurrently within the γ matrix during aging.[8] Additionally, depending on the chemical composition, aging temperature, and aging time, the wavelength was determined in the range of 23 to 35 nm.[6–9] In spite of the different propositions for the process of spinodal decomposition and ordering, it can generally be concluded that austenitic FeMnAlC alloys with $3.1 \leq C \leq 5.2$ at% also lay within the spinodal, and that spinodal decomposition and formation of ordered k′ particles can only be detected in the alloys during isothermal aging. However, in the present alloys with $5.5 \leq C \leq 8.0$ at%, spinodal decomposition and formation of ordered k′ particles could occur during quenching. The apparent difference may be attributed to the following two reasons: (I) the effect of strain energy between the k′ particles and γ_0 phase, as discussed above, and (II) the degree of carbon supersaturation in the initial γ phase. As mentioned above, the lattice modulation that occurred in the present alloys is mainly caused by concentration fluctuations in the carbon atom, and the lattice parameter of k′ particles increased with increasing carbon content of the alloy. The carbon concentration in k′ particles can be estimated using the equation:[15] $a_{k'} = 0.36626 + 0.00059C_x$, where the lattice parameter $a_{k'}$ and carbon concentration C_x are presented in nanometers and atomic percent, respectively. The calculated results are also listed in Table 1. It is clear from the table that by increasing the carbon content of the alloy from 5.5 to 8.0 at%, the carbon concentration in k′ particles gradually increased from 11.08 at% ($x = 0.50$) to 15.32 at% ($x = 0.73$). It is evident that a higher degree of carbon supersaturation in the initial γ phase would increase not only the amount of fine k′ particles but also the carbon concentration in the k′ particles. Interestingly, it is noted here that the carbon concentrations of 11.08–15.32 at% ($x = 0.50$–0.73) are comparable to the values of 9–13 at% ($x = 0.4$–0.66) reported by other workers in austenitic Fe-27–30 at% Mn-14–20 at% Al-3.7–5 at% C alloys aged at 500–550°C for longer periods of time.[6,9,11]

Finally, it is worth pointing out that no information concerning the spinodal decomposition curve of the FeMnAlC alloy system has been provided in the literature. Clearly, additional work is needed to further understand the effects of carbon content on spinodal decomposition and ordering in austenitic FeMnAlC alloys.

4. Conclusions

In summary, spinodal decomposition and formation of ordered k′ particles were observed in the present Fe-26 at%Mn-20 at%Al-C alloys with $5.5 \leq C \leq 8.0$ at% under the as-quenched condition. The gradual increase in both the wavelength and the amount of ordered k′ particles indicates that the reaction temperatures of both spinodal decomposition and ordering increased with increasing carbon content. With increasing carbon content, the lattice parameters of both the ordered k′ particles and the disordered γ_0 phase increased, whereas the misfit between the two phases decreased. The coherency strain energy was expected to increase dramatically as the carbon content approached slightly below 5.5 at%. Given the remarkable increase in strain energy, undercooling may be insufficient to overcome the strain energy effects, which are responsible for the absence of spinodal decomposition and formation of ordered k′ particles in the present alloy A (5 C) and in previous austenitic FeMnAlC alloys with $3.1 \leq C \leq 5.2$ at% under the as-quenched condition. Additionally, the carbon concentration in the k′ particles formed in the present alloys increased with increasing carbon content. This indicates that a higher degree of carbon supersaturation in the initial γ phase might promote a tendency toward C-rich k′ particle formation during quenching.

Acknowledgment

This work was supported by the National Science Council, Taiwan (NSC-97-2221-E-009-027-MY3).

REFERENCES

1) I. Kalashnikov, O. Acselrad, A. Shalkevich and L. C. Pereira: J. Mater. Eng. Perform. **9** (2000) 597–602.
2) K. H. Han: Mater. Sci. Eng. A **279** (2000) 1–9.
3) O. Acselrad, A. R. de Souza, I. S. Kalashnikov and S. S. Camargo Jr.: Wear **257** (2004) 999–1005.
4) K. H. Han, J. C. Yoon and K. W. Choo: Scr. Metall. **20** (1986) 33–36.
5) I. S. Kalashnikov, O. Acsrlrad, A. Shalkevich, L. D. Chumakova and L. C. Pereira: J. Mater. Process. Tech. **136** (2003) 72–79.
6) K. Sato, K. Tagawa and Y. Inoue: Metall. Trans. A **21A** (1990) 5–11.
7) K. H. Han, W. K. Choo and D. E. Laughin: Scr. Metall. **22** (1988) 1873–1878.
8) W. K. Choo, J. H. Kim and J. C. Yoon: Acta Mater. **45** (1997) 4877–4885.
9) K. Sato, K. Tagawa and Y. Inoue: Mater. Sci. Eng. A **111** (1989) 45–50.
10) G. S. Krivonogov, M. F. Alekseyenko and G. G. Solov'yeva: Fitz. Metal. Metalloved **39** (1975) 775–781.
11) N. A. Storchak and A. G. Drachinskaya: Fitz. Metal. Metalloved **44** (1977) 373–380.
12) C. S. Wang, C. N. Hwang, C. G. Chao and T. F. Liu: Scr. Mater. **57** (2007) 809–812.
13) D. A. Porter, K. E. Easterling and M. Sherif: *Phase Transformations in Metals and Alloys 3rd Ed.*, (Nelson Thornes Ltd, Cheltenham, 2009) pp308–314.
14) B. Ditchek and L. H. Schwartz: Acta Metall. **28** (1980) 807–822.
15) W. K. Choo and K. H. Han: Metal. Trans. A **16A** (1985) 5–10.